Pt, Zr, Ni-containing carbon nanofiber composites modified by self-phosphorylating polybenzimidazole as cathode materials for hydrogen-air high-temperature polymer-electrolyte membrane fuel cell

I. I. Ponomarev, *Doctor of Chemical Sciences, Head of Laboratory, Chief Researcher[1], e-mail: gagapon@ineos.ac.ru*
K. M. Skupov*, *PhD in Chemistry, Senior Researcher[1], e-mail: kskupov@ineos.ac.ru*
E. S. Vtyurina, *Master's Degree in Materials Science, Junior Researcher[1], e-mail: ves1809@yandex.ru*
O. M. Zhigalina, *Prof., Doctor of Physical-Mathematical Sciences, Leading Researcher[2], e-mail: zhigal@crys.ras.ru*

[1]A.N. Nesmeyanov Institute of Organoelement Compounds of Russian Academy of Sciences, Moscow, Russia.
[2]National Research Centre "Kurchatov Institute", Moscow, Russia.

High-temperature polymer-electrolyte membrane fuel cells (HT-PEMFCs) operate at 150–200 °C, making it possible to use hydrogen contaminated with carbon monoxide. However, the main drawback for their distribution is the need to improve stability of membrane-electrode assembly components, especially cathodes. The cathodes based on carbon nanofiber (CNF) mat are free-standing (self-supporting), and are prepared using the method of electrospinning from a polyacrylonitrile solution containing Zr and Ni salts, followed by the stabilization and pyrolysis steps. The composite Zr, Ni-containing Pt/CNF cathodes are obtained after Pt nanoparticle deposition on the CNF surface. A novel self-phosphorylating polybenzimidazole (PBI-6F) was deposited to the surface of Pt/CNF to improve the triple-phase boundary. Substitution of OMe-groups and hydrophobic nature of CF_3-groups lead to improvements in proton conductivity and gas transport of the cathode as well as proton-conducting contacts between cathode and membrane. The materials are studied using N_2 and CO_2 gas adsorption, TEM, HAADF STEM. The operation of the H_2/air HT-PEMFC shows that the application of the PBI-6F-covered PBI-6F/Pt/CNF cathode results in an enhancement of HT-PEMFC performance, compared with the uncovered Pt/CNF cathode, providing ~20% increase in maximum power density.

Key words: polybenzimidazole 6F, Pt nanoparticles, composite carbon nanofiber mat, self-phosphorylating polymer, Pt/CNF, HT-PEMFC, gas-diffusion electrode, carbon nanofiber, polyacrylonitrile.

DOI: 10.17580/nfm.2024.02.05

Introduction

The improvement of innovative electrode materials is of crucial importance for the advancement of hydrogen energy technology, particularly in the area of fuel cells (FCs) [1]. H_2/air high-temperature polymer-electrolyte (or proton-exchange) membrane fuel cells (HT-PEMFCs) on polybenzimidazole (PBI) membrane are of significant importance due to many advantages [2–24]. Their essential feature is the ability to operate with H_2, contaminated with CO, due to their operation at relatively high temperature (160–200 °C). The typical HT-PEMFC membrane-electrode assembly (MEA) consists of the *m*-PBI membrane and electrodes based on carbon black (CB) with deposited Pt nanoparticles [1]. Triple phase boundary formation is essential for the course of electrochemical reactions in the HT-PEMFC electrodes (anodes and cathodes) since it ensures the contacts of Pt electrocatalyst with electron-conducting phase (carbon material), proton-conducting phase (phosphoric acid) and gas channels [8]. Unfortunately, the CB-based electrodes are not sufficiently stable under conditions of HT-PEMFC operation (high potentials, H_3PO_4 medium, high temperatures). Therefore, it becomes necessary to replace CB with more stable materials, such as carbon nanostructured materials [25, 26], for example, carbon nanofibers (CNF). Earlier [27–29], we have developed Pt/CNF composite electrodes based on polyacrylonitrile (PAN) [30] or polymer of intrinsic microporosity [31]. Pt/CNF were produced by electrospinning [32–34] followed by pyrolysis [35] of nanofiber mats and deposition of Pt nanoparticles. Recently, to improve the HT-PEMFC MEA performance, we have developed self-phosphorylating membrane PBI-OMe [36] as well as proton-conducting polymer coatings for Pt/CNF anodes: PBI-OPhT-P [37] and self-phosphorylating PBI-6F [38]. PBI-6F can be obtained from PA-6F, during the cyclization procedure at ~300 °C and followed by the self-phosphorylation step **(Fig. 1)** [38].

According to our approach of self-phosphorylation which was previously presented in [36, 38], the MeO-groups can be substituted at ~180 °C, e.g., under typical HT-PEMFC operation conditions. Therefore, we have shown that anodes can be improved by PBI-6F deposition [38]. The improvement in the triple phase boundary formation is reached by better gas permeability due to PBI-6F hydrophobic properties on one hand, and proton conductivity of PBI-6F on the other.

*Correspondence author.

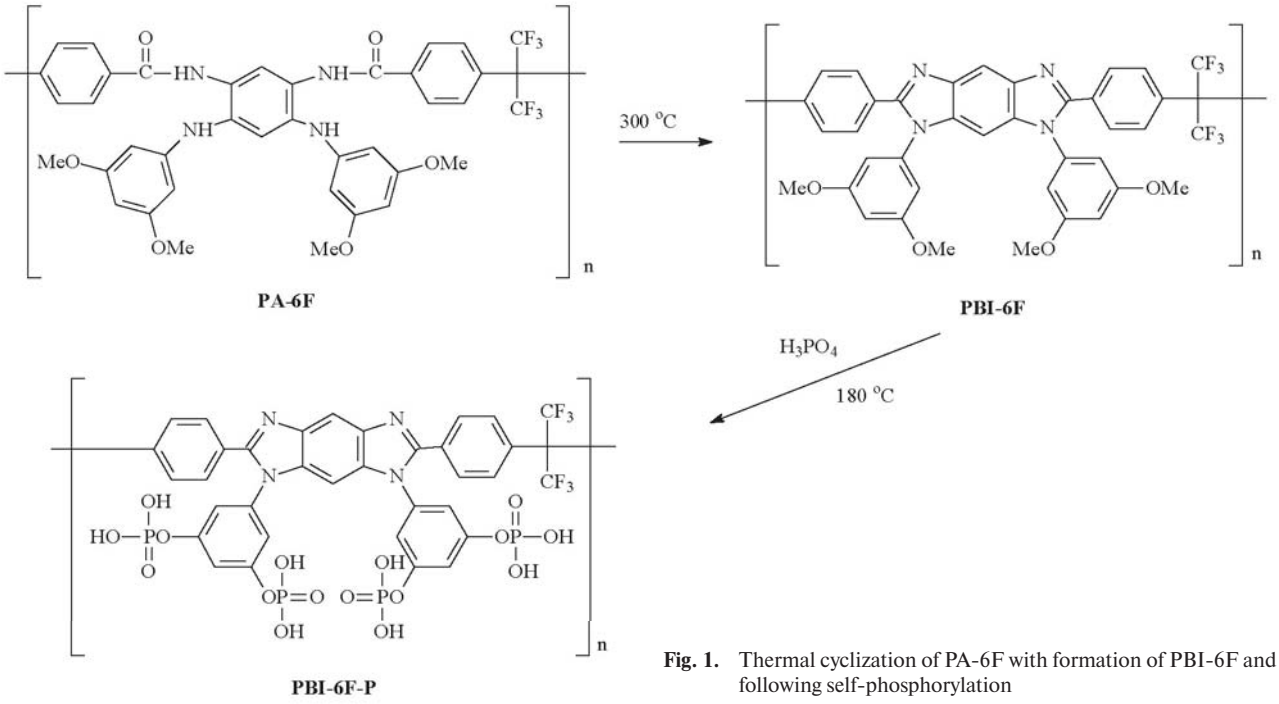

Fig. 1. Thermal cyclization of PA-6F with formation of PBI-6F and its following self-phosphorylation

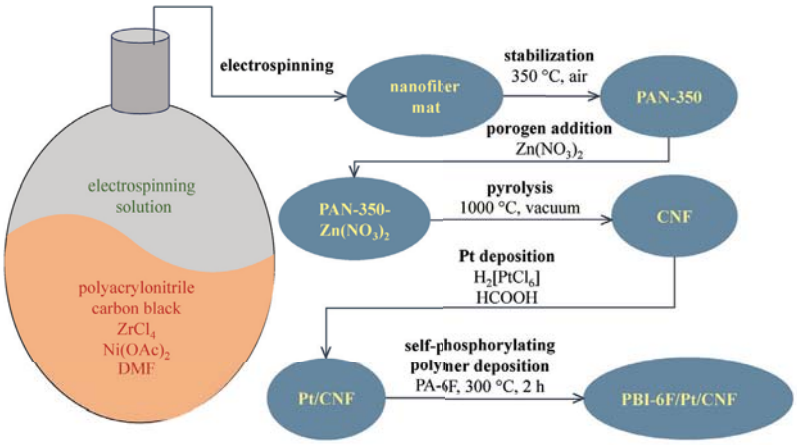

Fig. 2. A general scheme of the obtaining of Pt, Ni, Zr-containing composite Pt/CNF and PBI-6F/Pt/CNF cathodes

At the same time, the improvement of the cathodes in HT-PEMFCs is still a major challenge in achieving higher efficiencies.

The aim of this study is to increase the HT-PEMFC MEA performance by improving proton transport contacts using the PBI-6F coating for the cathode. In this study, for the first time, the self-phosphorylating PBI-6F coating was deposited onto composite carbonized Pt, Zr, Ni-containing CNF-based cathode, and tested in MEA for the H_2/air HT-PEMFC.

Materials and Methods

Zr, Ni-containing composite PAN-based nanofiber mat is obtained in accordance to the Nanospider^{TM} technology of needle-free (free surface) electrospinning on an Elmarco NS Lab NanospiderTM (Liberec, Czech Republic) at 69 kV (RH 8%). A typical electrospinning procedure follows. PAN (3.25 g, M_w 150 · 10^3 Da), Vulcan® XC-72 CB (0.1 g, ~3 wt.% relative to PAN), $Ni(OAc)_2$ (0.37 g), $ZrCl_4$ (0.03 g) are dispersed in N,N-dimethylformamide (50 mL) in ultrasonic bath (3 h). The nanofiber mat is stabilized at 350 °C (air, 2 h), immersed into $Zn(NO_3)_2$ solution (0.5 wt.%) in water/ethanol (1 : 3 v/v) for ~24 h, then dried (100 °C, 2 h). Finally, it is carbonized (pyrolyzed) at 1000 °C (2 h, vacuum, 3 K/min heating rate). T_b of Zn is 906 °C, therefore, when it evaporates, it forms a porous structure in the final carbonized composite CNF mat.

Pt deposition on a CNF mat with an area of 6.76 cm^2 is carried out in 10 mL of H_2O with the calculated amount of $H_2[PtCl_6] \cdot 6H_2O$ and 0.5 g of HCOOH (reducing agent) to obtain cathode electrocatalysts with Pt load of 1.2 mg_{Pt}/cm^2. The system is kept at room temperature for 3 days. The resulting Pt/CNF mat is obtained after washing with distilled water and drying (100 °C, 2 h, vacuum).

Self-phosphorylated proton-conducting PBI-6F polymer with a 6F-bridge group (obtained according to [38]) is deposited as a coating to the Pt/CNF mat by immersing Pt/CNF into 0.1 wt.% solution of PA-6F **(Fig. 1)** in hexafluoroisopropanol for 15 min, followed by drying in air of the PA-6F-coated Pt/CNF mat. Finally, after heat treatment under vacuum at 300 °C for 1 h (PA-6F converts to PBI-6F according to [38]), the resulting cathode, Pt/CNF coated by PBI-6F, is obtained. A general scheme of the obtaining of the initial Ni, Zr-containing composite CNF as well as Pt/CNF and PBI-6F/Pt/CNF cathodes is shown in **Fig 2**.

N_2 sorption-desorption isotherms are obtained in a range 10^{-3} – 1 bar at 77 K on a 3P Micro 200 Surface Area and Pore Size Analyzer (3P Instruments, Germany). The Brunauer–Emmett–Teller (BET) specific surface area (SSA) is calculated according to the BET equation, taking into account the Rouquerol criteria [39]. To obtain SSA, the Langmuir equation is also applied. Micropore SSA as well as SSA of meso- and macropores are found by the *t*-method using the Harkins-Jura equation [40, 41]. The adsorption layer thickness (*t*) range is 0.43–0.65 nm. CO_2 sorption-desorption isotherms are obtained in a range 10^{-3} – 1 bar at 273 K on a 3P Micro 200 Surface Area and Pore Size Analyzer (3P Instruments, Germany). The specific volume (SV) and SSA values and pore size distributions (PSD) are found by the non-local density functional theory (NLDFT) method using NovaWin, Quantachrome Instruments, version 11.04. The Dubinin-Radushkevich (DR) method is applied to find SV also. The saturated vapor pressure of the adsorbate (p_0) and adsorbed CO_2 density are taken as 3.485 MPa and 1.044 g/cm^3, respectively; CO_2 cross-sectional area is taken as 0.210 nm^2; the affinity coefficient β is taken as 0.35 [42].

The structure of the initial composite Zr, Ni- containing CNF as well as Pt/CNF and PBI-6F/Pt/CNF is investigated by transmission electron microscopy (TEM), scanning transmission electron microscopy with a high-angle annular dark-field detector (HAADF STEM) and energy-dispersive *X*-ray spectroscopy (EDX) elemental mapping using a Thermo Fisher Scientific Osiris (USA) equipped with a HAADF detector and Super-X EDX detection system based on Silicon Drift Detector technology. Electron microscope images are analyzed using Esprit (Esprit 2, USA), TIA (TIA 16, Siemens AG, Germany) and Digital Micrograph (GMS 3, USA). The samples are ultrasonicated in acetone for 20-30 min to separate fibers, the obtained suspensions are introduced onto Cu lacey carbon grids.

For testing the Pt/CNF and PBI-6F/Pt/CNF cathodes in HT-PEMFC, the MEAs (working area of 5 cm^2) are prepared. Except the aforementioned cathodes, the HT-PEMFC MEAs are operated with a typical Celtec®-P 1000 MEA anode [43] and a PBI-O-PhT membrane (previously prepared in our group [44–46]). HT-PEMFC operation is carried out at 160, 180 and 200 °C. The MEAs are tested in a standard testing cell (Arbin Instruments, USA) with two graphite flow field plates. The anode side is supplied with H_2 (100 mL/min) obtained by electrolysis from a Khimelektronika GVCh-6 hydrogen generator (Russia); and the cathode side is supplied

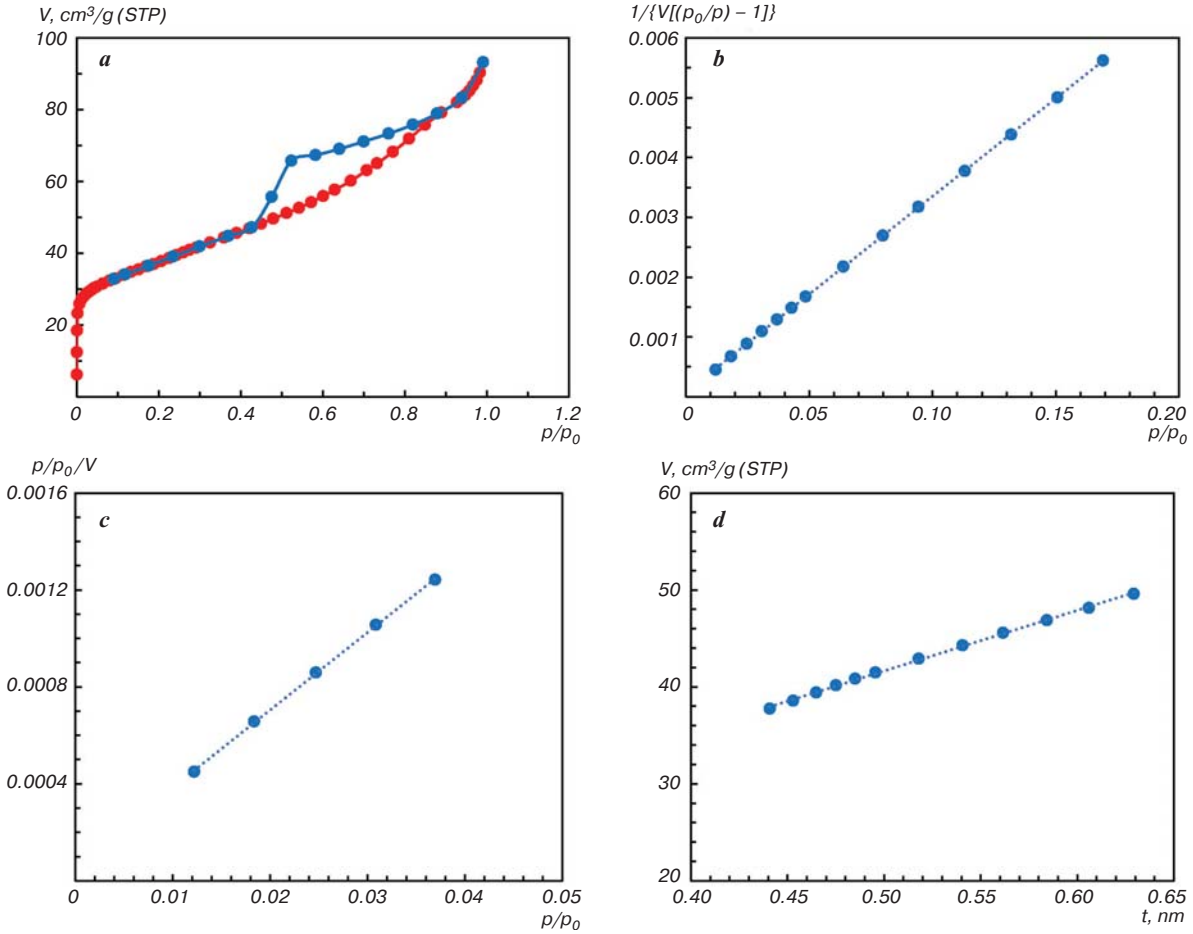

Fig. 3. (*a*) Low-temperature nitrogen sorption-desorption isotherms (77 K) for the CNF sample; (*b*) the corresponding BET plot; (*c*) Langmuir plot; (*d*) *t*-plot

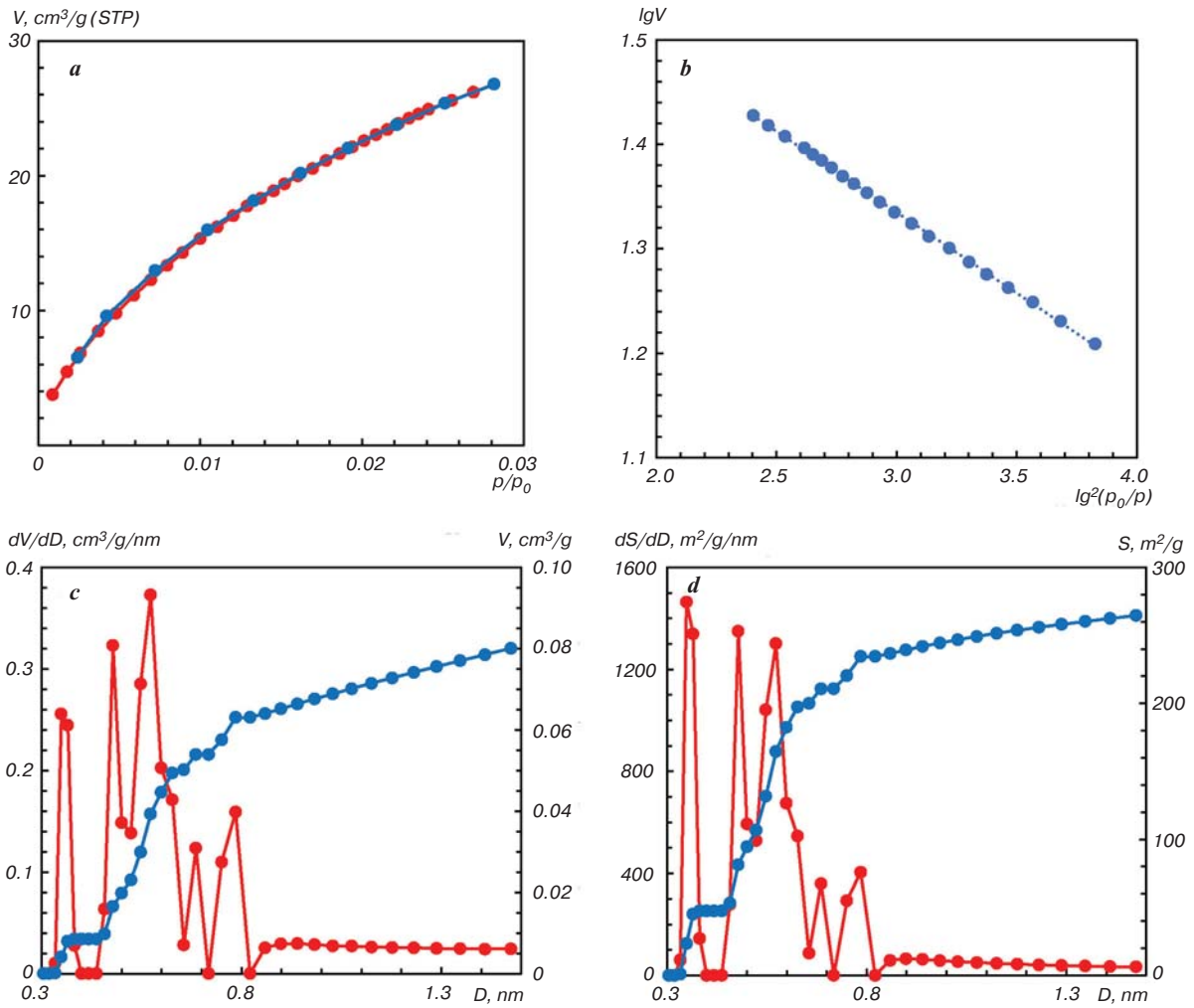

Fig. 4. (*a*) Carbon dioxide sorption-desorption isotherms (273 K) for the CNF sample; (*b*) the corresponding DR plot; (*c*) NLDFT pore size distrubition (*dV*/*dD*); (*d*) NLDFT pore size distrubition (*dS*/*dD*)

with atmospheric air without additional humidification (1000 mL/min). Electrochemical Instruments P-150X Potentiostat-galvanostat (Russia) is used to obtain the polarization curves.

Results and Discussion

The electrospinning solution, containing PAN, Vulcan XC-72, $ZrCl_4$, $Ni(OAc)_2$ in DMF is electrospun, then the resulting nanofiber mat is stabilized at 350 °C, impregnated with $Zn(NO_3)_2$ solution, dried and pyrolyzed at 1000 °C under vacuum. Since Zn boiling point is 906 °C, it evaporates providing porous structure to the resulting carbonized material. Finally, Ni and Zr are present in in a CNF mat in a form of Ni^0, which improves Pt electrocatalytic activity, and ZrO_x, which forms zirconium hydrogen phosphate with phosphoric acid under HT-PEMFC MEA operating conditions, as it was shown in our previous studies [27]. The resulting composite CNF mat is carbonized and becomes electrically conductive (29.86 S/cm) and may be applied as a carbonized support for Pt nanoparticle electrocatalyst (%C 80.4; %N 2.8; %H 1.1; %Ni 4.5; %Zr 0.3).

Before deposition of Pt nanoparticles onto CNF mat, SSA and SV of the obtained composite CNF material have been investigated by the low-temperature N_2 adsorption (77 K) and CO_2 adsorption (273 K). N_2 adsorption isotherm, BET plot, Langmuir plot and t-plot for the low-temperature N_2 adsorption on the composite CNF material are shown in **Fig. 3**.

As found from Fig. 3, the BET SSA value (S_{BET}) is 133 m^2/g. Alternatively, the Langmuir SSA value (S_{Lang}) is found to be 134 m^2/g, which is almost the same as S_{BET}. In order to differentiate between micropores ($D < 2$ nm), mesopores (D 2–50 nm) and macropores ($D > 50$ nm), the t-method was employed. Based on the t-plot data, the micropore SSA and micropore SV values are calculated to be 36 m^2/g and 0.016 cm^3/g, correspondingly, while the SSA value for meso- and macropores is found to be 97 m^2/g. The total SV is found to be 0.143 cm^3/g (at $p/p_0 = 0.990$) which corresponds to the average pore size ($4V/S$) of 4.3 nm. Albeit, this SSA is not especially high, it is sufficient for standard Pt nanoparticle deposition. A relatively low value of SSA of micropores (36 m^2/g) could be related to the inaccessibility of

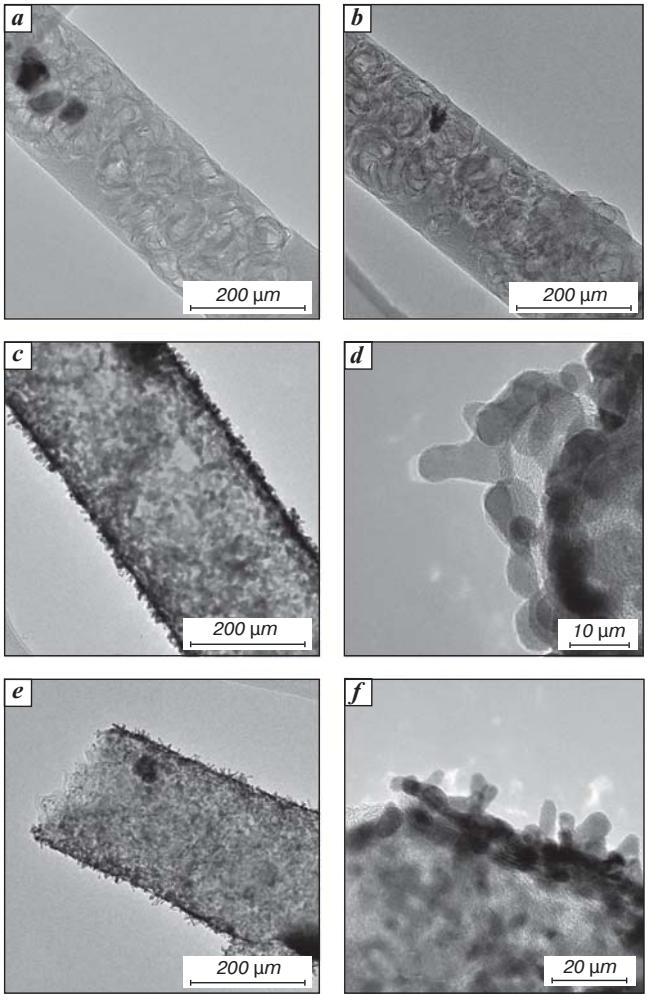

Fig. 5. The TEM images for composite CNF material (*a*, *b*); Pt/CNF (c, d); and PBI-6F/Pt/CNF (e, f) taken with higher (*b*, *d*, *f*) and lower (*a*, *c*, *e*) magnification

micropores for N_2 molecules at low temperature (77 K). To overcome these difficulties, the CO_2 adsorption was carried out at 273 K [47]. At 273 K the adsorbate molecules become more mobile and may enter the inaccessible micropores. CO_2 adsorption isotherm, DR plot and NL-DFT pore-size distribution of micropores is provided in **Fig. 4**.

As it follows from the CO_2 adsorption data according to NLDFT method, the SSA and SV values are 265 m^2/g and 0.080 cm^3/g. As follows from the PSD, ultramicropores (D < 0.7 nm) comprise the largest part of micropores which correspond to SSA of 211 m^2/g. The DR SV value is 0.119 cm^3/g which is a bit higher since different theoretical approaches are employed for these two methods, and larger in size micropores are taken into account in the DR method. Therefore, in addition to easily accessible meso- and micropores, the sample also contains a system of relatively closed micropores which are difficult to access.

Initial CNF material (before Pt deposition), Pt/CNF and PBI-6F/Pt/CNF are investigated by electron microscopy; HAADF STEM images, elemental map distributions and EDX spectra were also obtained **(Figs. 5, 6)**

As can be seen from **Fig. 5**, Ni presents in two forms, small uniformly distributed nanoparticles and large spherical nanoparticles up to 35 nm in diameter. It can be observed that graphitized carbon layers are located in areas around Ni nanoparticles. For samples with deposited Pt, it is seen that Pt nanoparticles are uniformly distributed throughout nanofiber's surface according to the Pt distribution map **(Fig. 6)**.

Pt nanoparticles exhibit spherical and needle-like (up to 20 nm in length) morphologies, as well as a mixture of these two morphologies changing in shape from one to another. Applying a self-phosphorylating PA-6F coating to the surface of Pt/CNF, followed by thermal treatment at 300 °C, results in the conversion of the material into PBI-6F, as previously explained, and the formation of a PBI-6F coating on the surface of Pt/CNF. The elemental distribution maps for F **(Fig. 6)** confirm the uniform distribution of F (and therefore of the PBI-6F coating) across the surface, which may lead to higher proton-conducting

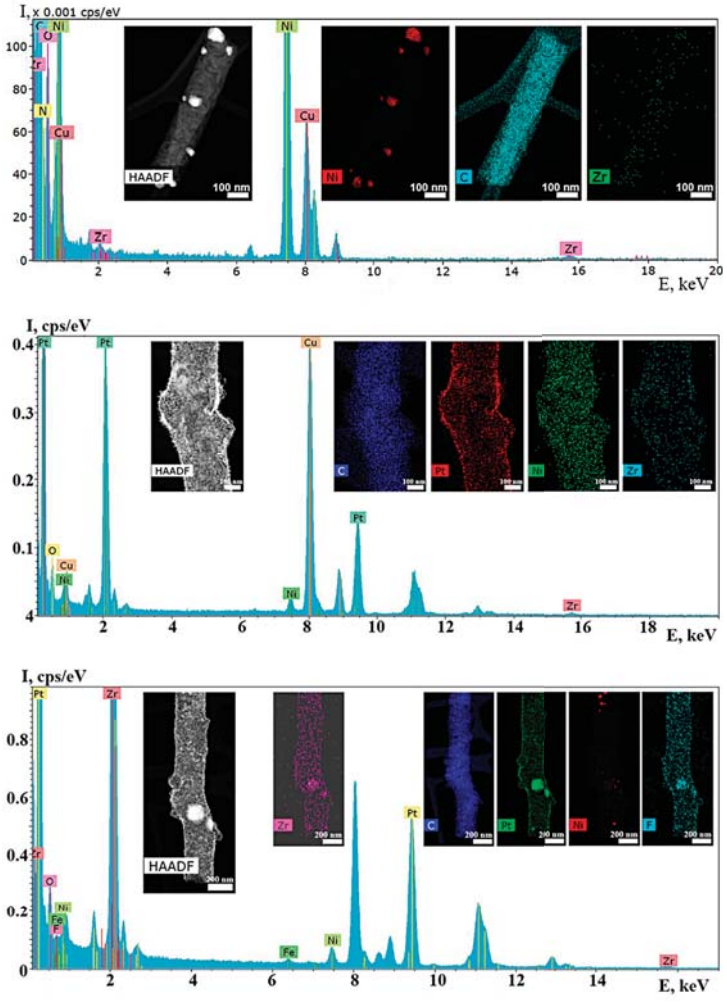

Fig. 6. EDX spectra with insertions of HAADF STEM images with elemental maps for composite CNF (top); Pt/CNF (center); and PBI-6F/Pt/CNF (bottom)

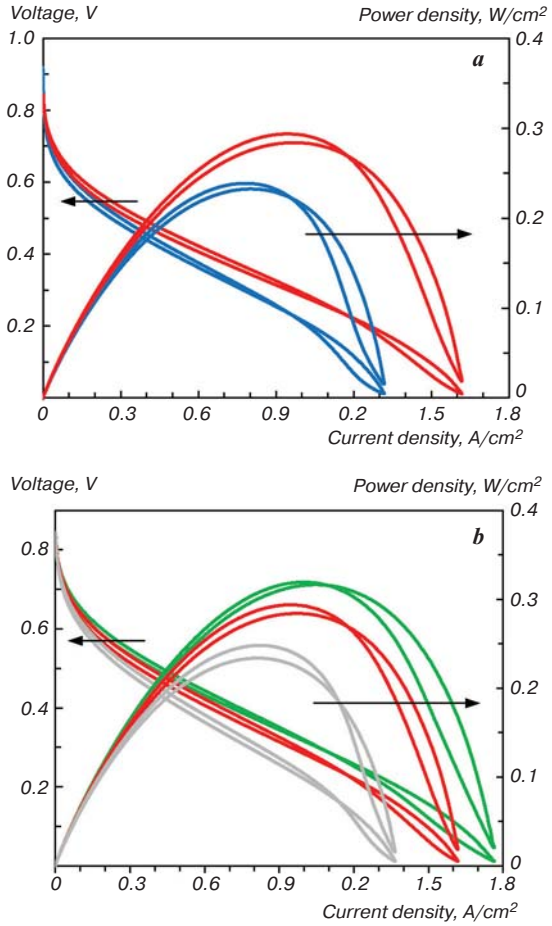

Fig. 7. (*a*) Polarization and power density curves (forward and reverse) at 180 °C for MEA with uncovered Pt/CNF cathode (blue) and MEA with PBI-6F/Pt/CNF cathode (red); (*b*) polarization and power density curves (forward and reverse) for MEA with PBI-6F/Pt/CNF cathode at 160 °C (grey), 180 °C (red) and 200 °C (green)

contacts and HT-PEM FC performance. Uniform distribution of F and Pt allows to employ this composite material as an HT-PEMFC cathode. The electrochemically active specific surface area values of Pt for Pt/CNF, uncovered and covered by the PBI-6F self-phosphorylating coating, are found to be 15–17 m^2/g_{Pt} which is satisfactory to apply them in the HT-PEM FC MEA. The performance of the HT-PEMFC was analyzed for MEAs which contained the PBI-O-PhT membrane, Celtec®P1000 anode, and PBI-6F-coated and uncoated composite Pt/CNF cathodes, at 160–200 °C based on polarization curve and power density curve data **(Fig. 7)**.

As can be seen from Fig. 7a, the MEA with the obtained PBI-6F/Pt/CNF cathode have an advantage over the non-coated one. At 180 °C, the maximum power density was increased to 294 mW/cm^2 at 0.95 A/cm^2 in the case of the PBI-6F-coated cathode compared with 239 mW/cm^2 at 0.82 A/cm^2 which is ~20 % higher than in the case of the uncoated cathode. Also, the maximum power density is achieved at higher current densities. Polarization curve shows higher voltage values in the case of the PBI-6F coated cathode compared with the case of the uncoated one (477 vs. 457 mV) at 0.4 A/cm^2. Temperature dependence of MEA performance is shown in Fig. 7b. The polarization and power density curves were recorded at 160, 180 and 200 °C. The voltage values at 0.4 A/cm^2 are increasing with temperature increase 458 mV (160 °C), 477 mV (180 °C), and 510 mV (200 °C). The maximum power densities become higher with the temperature increase and appear at higher current densities 248 mW/cm^2 at 0.83 A/cm^2 (160 °C), 294 mW/cm^2 at 0.95 A/cm^2 (180 °C), and 319 mW/cm^2 at 1.01 A/cm^2 (200 °C). The improved MEA performance is explained by two factors. The higher voltage and power density values, as well as the higher current densities achieved, can be attributed to better proton-conducting contacts between the proton-conducting membrane and GDE, which are facilitated by the self-phosphorylating PBI-6F coating. Additionally, the partial elimination of mass transfer of the reagents at higher current densities is due to the hydrophobic properties imparted to the PBI-6F coating by CF_3-groups which help to organize gas channels in the electrode better.

Conclusions

The improvement of HT-PEMFC MEA performance is achieved by modifying the Ni, Zr-containing composite Pt/CNF cathode surface by the self-phosphorylating polybenzimidazole-type (PBI-6F) coating compared with the case of the non-modified Pt/CNF cathode. Higher performance was reached due to better proton-conducting contacts between the proton-conducting membrane and gas-diffusion cathode. Another advantage of the PBI-6F coating is related to mass transfer facilitation due to better organization of gas channels in the carbon nanofiber cathode because of the hydrophobic properties imparted to the PBI-6F coating by the CF_3-groups. The improvement in proton conductivity resulting from the substitution of OMe-groups, better contacts between the gas diffusion electrode and the polymer-electrolyte membrane, and improved gas channel organization due to the hydrophobic CF_3-groups have a significant impact on enhancing the triple-phase boundary, providing ~20% increase in maximum power density for the HT-PEM FC performance.

The study was financially supported by Russian Science Foundation (grant # 22-13-00065). Elemental analysis was performed with support of Ministry of Science and Higher Education of the Russian Federation using the equipment of Center for Molecular Composition Studies of INEOS RAS. The authors would like to express their gratitude to D. N. Khmelenin and E. N. Cherkovskiy of NRC "KI" for their assistance with electron microscopy data; Yu. A. Volkova, Iv.I. Ponomarev and A. G. Buyanovskaya of INEOS RAS for their contributions to the membrane obtaining, electrospinning results and elemental analysis data; and A. D. Modestov of IPCE RAS for his assistance with electrochemistry data.

References

1. Li Q., Aili D., Hjuler H. A., Jensen J. O. High Temperature Polymer Electrolyte Membrane Fuel Cells. Approaches, Status, and Perspectives. Cham: Springer, 2016. XXVI+545 p. DOI: 10.1007/978-3-319-17082-4

2. Rosli R. E., Sulong A. B., Daud W. R. W., Zulkifley M A., Husaini T., Rosli M. I., Majlan E. H., Haque M. A. A Review of High-Temperature Proton Exchange Membrane Fuel Cell (HT-PEMFC) System. *International Journal of Hydrogen Energy*. 2017. Vol. 42. pp. 9293–9314. DOI: 10.1016/j.ijhydene.2016.06.211

3. Seselj N., Alfaro S. M., Bompolaki E., Cleemann L. N., Torres T., Azizi K., Catalyst Development for High-Temperature Polymer Electrolyte Membrane Fuel Cell (HT-PEMFC) Applications. *Advanced Materials*. 2023. Vol. 35. 2302207. DOI: 10.1002/adma.202302207

4. Authayanum S., Im-orb K., Arpornwichnop A. A Review of the Development of High Temperature Proton Exchange Membrane Fuel Cells. *Chinese Journal of Catalysis*. 2015. Vol. 36. pp. 473–483. DOI: 10.1016/S1872-2067(14)60272-2

5. Rasheed R. K. A., Liao Q., Caizhi Z., S. H. Chan. A Review of the Development of High Temperature Proton Exchange Membrane Fuel Cells. *International Journal of Hydrogen Energy*. 2017. Vol. 42. pp. 3142–3165. DOI: 10.1016/j.ijhydene.2016.10.078

6. Moorthy S., Sivasubramanian G., Kannaiyan D., Deivanayagam P. Neoteric Advancements in Polybenzimidazole Based Polymer Electrolytes for High-Temperature Proton Exchange Membrane Fuel Cells – A Versatile Review. *International Journal of Hydrogen Energy*. 2023. Vol. 48. pp. 28103–28118. DOI: 10.1016/j.ijhydene.2023.04.005

7. Li Q., He R., Jensen J. O., Bjerrum N. J. PBI-Based Polymer Membranes for High Temperature Fuel Cells – Preparation, Characterization and Fuel Cell Demonstration. *Fuel Cells*. 2004. Vol. 4. pp. 147–159. DOI: 10.1002/fuce.200400020

8. Zeis R. Materials and Characterization Techniques for High-Temperature Polymer Electrolyte Membrane Fuel Cells. *Beilstein Journal of Nanotechnology*. 2015. Vol. 6. pp. 68–83. DOI: 10.3762/bjnano.6.8

9. Zhou Z., Zholobko O., Wu X.-F., Aulich T., Thakare J., Hurley J. Polybenzimidazole-Based Polymer Electrolyte Membranes for High-Temperature Fuel Cells: Current Status and Prospects. *Energies*. 2021. Vol. 14. 135. DOI: 10.3390/en14010135

10. Escorihuela J., Olvera-Mancilla J., Alexandrova L., del Castillo L.F., Compañ V. *Polymers*. Recent Progress in the Development of Composite Membranes Based on Polybenzimidazole for High Temperature Proton Exchange Membrane (PEM) Fuel Cell Applications. Polymers. 2020. Vol. 12. 1861. DOI: 10.3390/polym12091861

11. Rath R., Kumar P., Unnikrishnan L., Mohanty S., Nayak S. K. Current Scenario of Poly (2,5-Benzimidazole) (ABPBI) as Prospective PEM for Application in HT-PEMFC. *Polymer Review*. 2019. Vol. 60. pp. 267–317. DOI: 10.1080/15583724.2019.1663211

12. Pingitore A. T., Molleo M., Schmidt T. J., Benicewicz B. C. Polybenzimidazole Fuel Cell Technology: Theory, Performance, and Applications. In: *Encyclopedia of Sustainability Science and Technology* (Ed. by R. Meyers). New York: Springer, 2018. pp. 1–38. DOI: 10.1007/978-1-4939-2493-6_143-3

13. Quartarone E., Angioni S., Mustarelli P. Polymer and Composite Membranes for Proton-Conducting, High-Temperature Fuel Cells: A Critical Review. *Materials*. 2017. Vol. 10. 687. DOI: 10.3390/ma10070687

14. Bose S., Kuila T., Nguyen T. X. H., Kim N. H., Lau K., Lee J. H. Polymer Membranes for High Temperature Proton Exchange Membrane Fuel Cell: Recent Advances and Challenges. *Progress in Polymer Science*. 2011. Vol. 36. pp. 813–843. DOI: 10.1016/j.progpolymsci.2011.01.003

15. Li Q., Jensen J. O., Savinell R. F., Bjerrum N. J. High Temperature Proton Exchange Membranes Based on Polybenzimidazoles for Fuel Cells. *Progress in Polymer Science*. 2009. Vol. 34. 449–477. DOI: 10.1016/j.progpolymsci.2008.12.003

16. Yaroslavtsev A. B., Stenina I. A. Current Progress in Membranes for Fuel Cells and Reverse Electrodialysis. *Mendeleev Communications*. 2021. Vol. 31. pp. 423–432. DOI: 10.1016/j.mencom.2021.07.001

17. Mader J., Xiao L., Schmidt T. J., Benicewicz B. C. Polybenzimidazole/Acid Complexes as High-Temperature Membranes. In: *Fuel Cells II. Advances in Polymer Science, vol. 216* (Ed. by G. G. Scherer). Berlin: Springer, 2008. pp. 63–124. DOI: 10.1007/12_2007_129

18. Zucconi A., Hack J., Stocker R., Suter T. A. M., Rettie A. J. E., Brett D. J. L. Challenges and Opportunities for Characterisation of High-Temperature Polymer Electrolyte Membrane Fuel Cells: a Review. *Journal of Materials Chemistry A*. 2024. Vol. 12. pp. 8014–8064. DOI: 10.1039/d3ta06895a

19. Subianto S. Recent Advances in Polybenzimidazole/Phosphoric acid Membranes for High-Temperature Fuel Cells. *Polymer International*. 2014. Vol. 63. pp. 1134–1144. DOI: 10.1002/pi.4708

20. Li G., Kujawski W., Rynkowska E. Advancements in Proton Exchange Membranes for High-Performance High-temperature Proton Exchange Membrane Fuel Cells (HT-PEMFC). *Reviews in Chemical Engineering*. 2022. Vol. 38. 327. DOI: 10.1515/revce-2019-0079

21. Kalathil A., Raghavan A., Kandasubramanian B. Polymer Fuel Cell Based on Polybenzimidazole Membrane: a Review. *Polymer-Plastics Technology and Materials*. 2019. Vol. 58. pp. 465–497. DOI: 10.1080/03602559.2018.1482919

22. Aili D., Henkensmeier D., Martin S., Singh B., Hu Y., Jensen J. O., Cleemann L. N., Li Q. Polybenzimidazole-Based High-Temperature Polymer Electrolyte Membrane Fuel Cells: New Insights and Recent Progress. *Electrochemical Energy Reviews*. 2020. Vol. 3. pp. 793–845. DOI: 10.1007/s41918-020-00080-5

23. Araya S. S., Zhou F., Liso V., Sahlin S. L., Vang J. R., Thomas S., Gao X., Jeppesen C., Kær S. K. A Comprehensive Review of PBI-Based High Temperature PEM Fuel Cells. *International Journal of Hydrogen Energy*. 2016. Vol. 41. pp. 21310–21344. DOI: 10.1016/j.ijhydene.2016.09.024

24. Haider R., Wen Y., Ma Z.-F., Wilkinson D. P., Zhang L., Yuan X., Song S., Zhang J. High Temperature Proton Exchange Membrane Fuel Cells: Progress in Advanced Materials and Key Technologies. *Chemical Society Reviews*. 2021. Vol. 50. pp. 1138–1187. DOI: 10.1039/D0CS00296H

25. Wang X. X., Tan Z. H., Zeng M., Wang J. N. Carbon Nanocages: A New Support Material for Pt Catalyst with

Remarkably High Durability. *Scientific Reports*. 2014. Vol. 4. 4437. DOI: 10.1038/srep04437

26. Shao Y., Liu J., Wang Y., Lin Y. Novel Catalyst Support Materials for PEM Fuel Cells: Current Status and Future Prospects. *Journal of Materials Chemistry*. 2009. Vol. 19. pp. 46–59. DOI: 10.1039/b808370c

27. Vtyurina E. S., Ponomarev I. I., Naumkin A. V., Bukalov S. S., Aysin R. R., Ponomarev I. I., Zhigalina O. M., Khmelenin D. N., Skupov K. M. Influence of the Polymer Precursor Structure on the Porosity of Carbon Nanofibers: Application as Electrode in High-Temperature Proton Exchange Membrane Fuel Cells. *ACS Applied Nano Materials*. 2024. Vol. 7. pp. 4313–4323. DOI: 10.1021/acsanm.3c05874

28. Skupov K. M., Ponomarev I. I., Vol'fkovich Y. M., Modestov A. D., Ponomarev Iv. I., Volkova Yu. A., Razorenov D. Yu., Sosenkin V. E. The Effect of the Stabilization and Carbonization Temperatures on the Properties of Microporous Carbon Nanofiber Cathodes for Fuel Cells on Polybenzimidazole Membrane. *Polymer Science, Series C*. 2020. Vol. 62. pp. 231–237. DOI: 10.1134/S1811238220020149

29. Vtyurina E. S., Skupov K. M., Ponomarev I. I., Buyanovskaya A. G., Ponomarev Iv. I., Zhigalina O. M., Cherkovskiy E. N., Khmelenin D. N. Carbon Nanofiber Gas-Diffusion Anodes Based on a Copolymer of Acrylonitrile with Methyl Acrylate for High-Temperature Polymer-Electrolyte Membrane Fuel Cell. *Protection of Metals and Physical Chemistry of Surfaces*. 2024. Vol. 60. pp. 100–109. DOI: 10.1134/S207020512470151X

30. Kopeć M., Lamson M., Yuan R., Tang C., Kruk M., Zhong M., Matyjaszewski K., Kowalewski T. Polyacrylonitrile-Derived Nanostructured Carbon Materials. *Progress in Polymer Science*. 2019. Vol. 92. pp. 89–134. DOI: 10.1016/j.progpolymsci.2019.02.003

31. Low Z.-X., Budd P. M., McKeown N. B., Patterson D. A. Gas Permeation Properties, Physical Aging, and Its Mitigation in High Free Volume Glassy Polymers. *Chemical Reviews*. 2018. Vol. 118. pp. 5871–5911. DOI: 10.1021/acs.chemrev.7b00629

32. Dong Z., Kennedy S. J., Wu Y. Electrospinning Materials for Energy-Related Applications and Devices. *Journal of Power Sources*. 2011. Vol. 196. pp. 4886–4904. DOI: 10.1016/j.jpowsour.2011.01.090

33. Inagaki M., Yang Y., Kang F. Carbon Nanofibers Prepared via Electrospinning. *Advanced. Materials*. 2012. Vol. 24. pp. 2547–2566. DOI: 10.1002/adma.201104940

34. Tenchurin T. Kh., Krasheninnikov S. N., Orekhov A. S., Chvalun S. N., Shepelev A. D., Belousov S. I., Gulyaev A. I. Rheological Features of Fiber Spinning from Polyacrylonitrile Solutions in an Electric Field. Structure and Properties. *Fibre Chemistry*. 2014. Vol. 46. pp. 151–160. DOI: 10.1007/s10692-014-9580-y

35. Yusof N., Ismail A.F. Post Spinning and Pyrolysis Processes of Polyacrylonitrile (PAN)-Based Carbon Fiber and Activated Carbon Fiber: A Review. *Journal of Analytical and Applied Pyrolysis*. 2012. Vol. 93. pp. 1–13. DOI: 10.1016/j.jaap.2011.10.001

36. Ponomarev I. I., Razorenov D. Y., Skupov K. M., Ponomarev I. I., Volkova Y. A., Lyssenko K. A., Lysova A. A., Vtyurina E. S., Buzin M. I., Klemenkova Z. S. Self-Phosphorylated Polybenzimidazole: An Environmentally Friendly and Economical Approach for Hydrogen/Air High-Temperature Polymer-Electrolyte Membrane Fuel Cells. *Membranes*. 2023. Vol. 13. 552. DOI: 10.3390/membranes13060552

37. Skupov K. M., Ponomarev I. I., Vtyurina E. S., Volkova Y. A., Ponomarev I. I., Zhigalina O. M., Khmelenin D. N., Cherkovskiy E. N., Modestov A. D. Proton-Conducting Polymer-Coated Carbon Nanofiber Mats for Pt-Anodes of High-Temperature Polymer-Electrolyte Membrane Fuel Cell. *Membranes*. 2023. Vol. 13. 479. DOI: 10.3390/membranes13050479

38. Ponomarev I. I., Volkova Y. A., Skupov K. M., Vtyurina E. S., Ponomarev I. I., Ilyin M. M., Nikiforov R. Y., Alentiev A. Y., Zhigalina O. M., Khmelenin D. N., Strelkova T. V., Modestov A. D. Unique Self-Phosphorylating Polybenzimidazole of the 6F Family for HT-PEM Fuel Cell Application. *International Journal of Molecular Science*. 2024. Vol. 25. 6001. DOI: 10.3390/ijms25116001

39. Rouquerol J., Rouquerol F., Sing K. S. W., Llewellyn P., Maurin G. Adsorption by Powders and Porous Solids: Principles, Methodology and Applications, 2nd ed. Cambridge: Academic Press, 2012. 626 p. DOI: 10.1016/C2010-0-66232-8

40. Harkins W. D., Jura G. Surfaces of Solids. XII. An Absolute Method for the Determination of the Area of a Finely Divided Crystalline Solid. *Journal of the American Chemical Society*. 1944. Vol. 66. pp. 1362–1366. DOI: 10.1021/ja01236a047

41. Choma J., Jaroniec M., Kloske M. Improved Pore-Size Analysis of Carbonaceous Adsorbents. *Adsorption Science & Technology*. 2002. Vol. 20. pp. 307–315. DOI: 10.1260/026361702760254487

42. Linares-Solano A., Stoeckli F. Commentary on the Paper "On the Adsorption Affinity Coefficient of Carbon Dioxide in Microporous Carbons" by E.S. Bickford et al. (Carbon 2004; 42: 1867–71). *Carbon*. 2005.Vol. 43. pp. 658–660. DOI: 10.1016/j.carbon.2004.10.007

43. Schmidt T. J., Baurmeister J. Properties of High-Temperature PEFC Celtec®-P 1000 MEAs in Start/Stop Operation Mode. *Journal of Power Sources*. 2008. Vol. 176. pp. 428–434. DOI: 10.1016/j.jpowsour.2007.08.055

44. Kondratenko M. S., Ponomarev I. I. Gallyamov M. O. Razorenov D. Y. Volkova Y. A., Kharitonova E. P., Khokhlov A. R. Novel Composite Zr/PBI-O-PhT Membranes for HT-PEFC Applications. *Beilstein Journal of Nanotechnology*. 2013. Vol. 4. pp. 481–492. DOI: 10.3762/bjnano.4.57

45. Ponomarev I. I., Skupov K. M., Modestov A. D., Lysova A. A., Ponomarev I. I., Vtyurina E.S. Cardo Polybenzimidazole (PBI-O-PhT) Based Membrane Reinforced with m-Polybenzimidazole Electrospun Nanofiber Mat for HT-PEM Fuel Cell Applications. *Membranes*. 2022. Vol. 12. 956. DOI: 10.3390/membranes12100956

46. Ponomarev I. I., Razorenov D. Y., Ponomarev I. I., Volkova Y. A., Skupov K. M., Lysova A. A., Yaroslavtsev A. B., Modestov A. D., Buzin M. I., Klemenkova Z. S. Polybenzimidazoles via Polyamidation: A More Environmentally Safe Process to Proton Conducting Membrane for Hydrogen HT-PEM Fuel Cell. *European Polymer Journal*. 2021. Vol. 156. 110613. DOI: 10.1016/j.eurpolymj.2021.110613

47. Lozano-Castello D., Cazorla-Amorós D., Linares-Solano A. Usefulness of CO_2 Adsorption at 273 K for the Characterization of Porous Carbons. *Carbon*. 2004. Vol. 42. pp. 1233–1242. DOI: 10.1016/j.carbon.2004.01.037